ACS OMEGA

http://pubs.acs.org/journal/acsodf

Article

Conductive Properties of Polyester/Spandex Fabrics Using Liquid Carbon Black and Disperse Black Dye

Li Ai, Shanshan Li, Hongmei Cao,* and Yawei Zhu

Cite This: *ACS Omega* 2023, 8, 4106−4115

Read Online

ACCESS | Metrics & More | Article Recommendations

ABSTRACT: Carbon black (CB) has been widely used in many fields; because the color depth of CB is not as good as dyes, black depth and color fastness cannot meet the requirements of users. Therefore, the application of CB in the textile field is greatly restricted. For this purpose, in this paper, we prepared liquid DB@CB (disperse black dye (DB)-modified carbon black) using mixed milling of CB and DB (consisting of Disperse Blue 79, Disperse Orange 288, and Disperse Violet 93). Using the dip-dry-bake method, polyester/spandex fabrics with excellent color fastness, deep black color, and good electrical conductivity were prepared. The rheological properties and interactions of CB and DB were studied by rheometer and transmission electron microscopy (TEM), the effects of DB@CB concentration on fabric resistance and electrical conductivity were investigated, the properties of DB@CB dyed fabrics were characterized by scanning electron microscopy (SEM) and X-ray photoelectron spectroscopy (XPS), and the stability and conductivity mechanism of liquid DB@CB were analyzed. The results showed that the liquid DB@CB was a pseudoplastic fluid based on strong intermolecular interaction by repulsive forces of CB and attractive forces of DB, improving the ordered arrangement and stability of CB and DB molecules. The liquid DB@CB showed a two-dimensional lamellar structure with a vortex-shaped helical molecular arrangement between CB and DB. The polyester/spandex fabrics dyed with DB@CB, had polygonal crystal structures and $\pi-\pi^*$ intermolecular interactions. It not only improved the conductivity of the fabric but also shows excellent color fastness, which can meet the application requirements of textiles and apparel for deep black, conductivity, and color fastness.

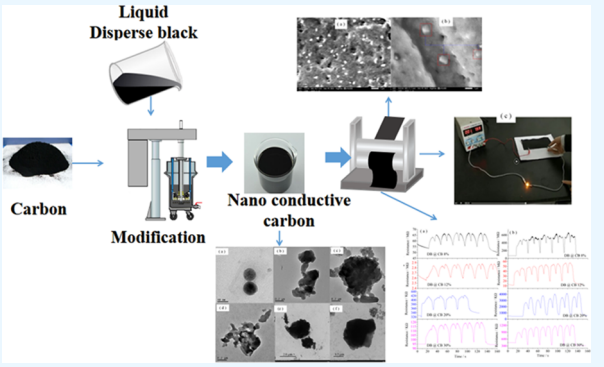

1. INTRODUCTION

Carbon-based materials, for example, carbon black (CB), carbon nanotube (CNT) (single-walled carbon nanotube and multiwalled carbon nanotube), graphene, etc., are environmentally friendly materials and have become important.[1] It has been widely used in paint, coating, tires, functional textile, and other fields. CB, which is widely available, easy to prepare, and inexpensive, has received a great deal of attention from researchers. CB can be used extremely versatile in the treatment of dye wastewater pollution, such as a conductive alkali-activated-steel-slag-magnesium-slag-based composite cementitious material (CACCM) could improve the photocatalytic degradation rate of the composite cementitious material.[2] CB can be used as a catalyst to improve catalytic efficiency, such as CB coupled into the interfaces between g-C_3N_4 and NiS photocatalysts exhibited the highest H-2-evolution rates using a simple precipitation method,[3] and the tin monoxide (SnO)@CB nanoparticles has better activity than other Sn catalysts for application in CO_2 reduction, while the high selectivity is attributed to a local pH effect arising from the dense packing of nanoparticles in the conductive CB matrix.[4] CB, like other carbon materials, is widely used as a filler in polymer matrices and as a finishing agent for surface material modification, the conductive behavior of CB is mainly governed by the increasing particle contact area and a limited effect of the surfactant on the conductivity.[5] Polymer/carbon based composites can be prepared as electromagnetic interference shielding materials.[6] Cotton fabrics coated with conductive CB, poly(vinyl alcohol), and natural rubber latex can be prepared with electromagnetic interference shielding and electrical conductivity.[7] Polyaniline-coated sulfur/conductive CB (PANI@S/C) composite has a high-rate charge/discharge capability due to a synergistic effect on the high electrical conductivity from both the conductive CB in the matrix and the PANI on the surface.[8] CB has great potential in wearable electronic devices for human motion detection, health monitoring, and other stretchable strain sensors. Thin CB-doped poly(dimethylsiloxane) (CB-PDMS) is used as a

Received: November 2, 2022
Accepted: January 5, 2023
Published: January 16, 2023

https://doi.org/10.1021/acsomega.2c06993
ACS Omega 2023, 8, 4106−4115

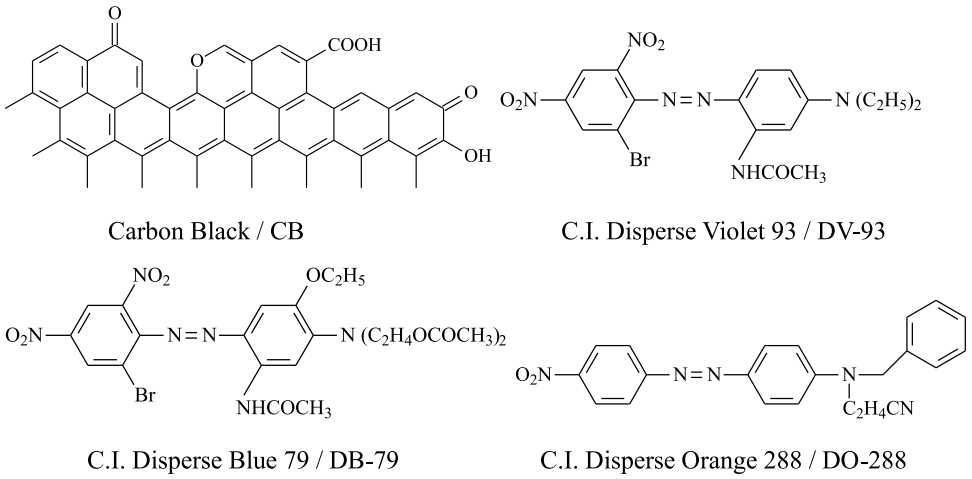

Figure 1. Structural formulas of carbon black and disperse dye.

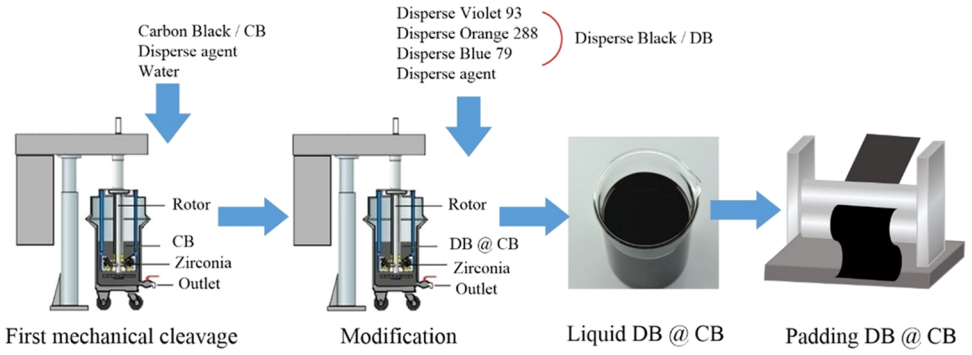

Figure 2. Diagram of liquid DB@CB preparation and application.

strain gauge due to its high resistivity and strong dependence on strain.[9] The fabricated versatile pressure sensors, based on microcrack-designed CB (CB@polyurethane) sponge via natural polymer-mediated water-based layer-by-layer assembly, exhibit excellent flexibility and fast response times.[10] A simple and facile solution mixing-casting method is adopted to fabricate a highly stretchable strain sensor based on composites mixing poly(dimethylsiloxane) (PDMS) with hybrid carbon nanotubes (CNTs) and CB conductive nanofillers (CNTs-CB).[11] The flexible and wearable strain conductive sensors are fabricated by mixing matrix poly(dimethylsiloxane) (PDMS) with zero-dimensional conductive filler CB.[12]

The application of CB in textile and clothing fabrics is mostly limited to electrical conductivity, electromagnetic shielding, anti-static, and anti-ultraviolet applications.[13−16] This is related to the shortcomings of the light color of CB in textile fibers and the uneven distribution of CB on the fabric, which is difficult to meet the requirements of functional clothing fabrics. The electrical conductivity of CB is more dependent on the increase in the particle contact area, the preparation of CB, modification methods, surface polar groups, and its microcrystalline structure.

The biggest disadvantage of CB for textile applications is the lack of black depth and good color fastness. This research solves this problem by preparing liquid DB@CB by combining CB and disperse dye black (DB), where DB is C.I. Disperse Blue 79 (DB-79), C.I. Disperse Orange 288 (DO-288), and C.I. Dispersing purple 93 (DV-93) complex. The rheological properties and interactions of CB and DB were studied to investigate their stability. Meanwhile, using the pad-dry-bake method, its effect on the electrical conductivity of polyester/spandex fabric was studied by finishing it on fabric. And the conductive mechanism of DB@CB was elaborated, and dyed fabrics with electrical conductivity and deep black color were prepared. This research provides a nonpolluting and low-cost application of CB in textiles and a practical reference for new uses of CB.

2. MATERIALS AND METHODS

2.1. Materials. The polyester/spandex fabrics were supplied by Jiangsu Wuxi Zhihong Textile Co. LTD. (Jiangsu, China). The fabric was warp knitted fabrics (92% 8.33 tex polyester fabric, 8% 4.44 tex spandex fabric, 320.0 g/m^2). The power carbon black (N330) was supplied by Anhui Black Cat Material Science Co., Ltd. (Anhui, China). The power disperse dye of C.I. Disperse Blue 79, C.I. Disperse Orange 288, and C.I. Disperse Violet 93 was supplied by Zhejiang Wanfeng Chemical Co., Ltd. (Zhejiang, China). The structure of disperse dyes is shown in Figure 1. The disperse agent of DE-22 (a mixture of anionic and nonionic dispersant and emulsion) and the adhesive agent of AE-20 were supplied by Suzhou Changchunteng Import and Export Co. Ltd. (Jiangsu, China).

2.2. Preparation of Liquid DB@CB. *2.2.1. Liquid DB@CB.* First, carbon black (CB, 25.0 g), DE-22 (9.5 g), and deionized water (50.0 g) were mixed and continuously ground with a vertical zirconium mill (2000 rpm) for 120 min. Then, to the above solution were added disperse blue 79 (4.7 g),

https://doi.org/10.1021/acsomega.2c06993
ACS Omega 2023, 8, 4106−4115

disperse orange 288 (5.4 g), disperse violet 93 (2.5 g), DE-22 (3.0 g), and continuously grinding (2000 rpm) for 90 min. Liquid DB@CB was made by filtration (shown in Figure 2).

2.2.3. Liquid Disperse Black Dyes (DB). It was prepared by combining disperse blue 79 (13.3 g), disperse orange 288 (15.4 g), disperse violet 93 (7.0 g), DE-22 (14.3 g), deionized water (50.0 g), and continuously grinding (2000 rpm) for 120 min.

2.2.4. Liquid CB. It was prepared by combining carbon black (CB, 25.0 g), DE-22 (9.5 g), and deionized water (65.5 g) and continuously grinding (2000 rpm) for 120 min.

The liquid Disperse Blue 79 (DB-79), Disperse Orange 288 (DO-288), and Disperse Violet 93 (DV-93) were prepared in the same way as DB.

The rheology of liquid dyes was tested on a Rheolab QC rotational rheometer (Austria Anton-Paar China Co., Ltd., Shanghai, China). The test conditions were 0 # rotor, temperature 20 °C, and shear rate 0.1−1000 s^{-1}. The shear stress (y, Pa) and shear rate (x, s^{-1}) were analyzed using a linear equation (eq 1), and the viscosity (y, mPa·s) and shear rate (x, s^{-1}) were analyzed using the Morgan−Mercer−Florin model (eq 2).

$$y = C_1 + C_2 x \quad (1)$$

$$y = (C_3 \times C_4 + C_5 \times x^{C_6})/(C_4 + x^{C_6}) \quad (2)$$

The transmission electron microscopy (TEM) was tested on an H-9500E TEM (Hitachi, Ltd., Tokyo, Japan) or an FEI Tecnai F20 TEM (FEI, Ltd.). The purpose is to observe the interaction of the dye, carbon black, and dispersant.

2.3. Dyeing of Polyester/Spandex Fabrics. The liquid DB@CB, adhesive agent AE-20 (5% of the mass of CB), and deionized water were prepared into the dye solution, polyester/spandex fabrics were impregnated, padded (100 ± 2% pick-up, shown in Figure 2), dried (80 °C), and thermally set (at 180 °C for 90 s).

The color characteristic values (L^*, a^*, b^*) were measured on a spectrophotometer (Ultra Scan XE, Hunter-Lab., Reston, VA) with a D_{65} light source and a 10° field of view. Here, L^* indicates the degree of color depth (the smaller the L value, the darker the color); a^* indicates the degree of reddish ($+a^*$) and greenish ($-a^*$); and b^* indicates the degree of yellowish ($+b^*$) and bluish ($-b^*$).

The fastness to rubbing of dyed fabrics was measured according to the standard (ISO105-171x12:2016) using a friction fastness machine (model 670, James H. Heal & Co. Ltd., Halifax, U.K.).

The washing fastness test was measured according to the standard (ISO105-C02:2013) using a wash fastness tester (Roaches International Co., Leek, Staffordshire, England).

Fabric resistance was measured on a source meter (Keithley Source meter 3465, Keithley). Stretch deformation and stretch rates were 30% and 48.75 mm/min, respectively.

Fabric electrical conductivity was measured according to the standard (GB/T 1551−2021) using a four-point probe tester (ST2258C, Suzhou Jingge Electronic Co., Ltd. Jiangsu, China). The test conditions were 20 °C, 65% RH, and 24 h sample equilibration.

Scanning electron microscopy (SEM) was performed on an S-4800 SEM (Hitachi, Ltd., Tokyo, Japan) under the condition that the surface of the fabric was sprayed with gold twice and the surface morphology of the fabric was observed under the accelerating voltage of 5 kV.

X-ray photoelectron spectroscopy (XPS) was tested on an ESCALAB 250 XPS (Thermo, Waltham, MA), using Al Kα radiation ($h\nu$ = 1486.6 eV) operated at 14.0 kV and 200 W.

3. RESULTS AND DISCUSSION

3.1. Rheology of Liquid Disperse Dye and Carbon Black. Figure 3 shows the rheology of the liquid disperse black dye (DB), carbon black (CB), and a mixture of DB and CB (DB@CB) (the samples of DB, CB, and DB@CB were prepared according to Section 2.2).

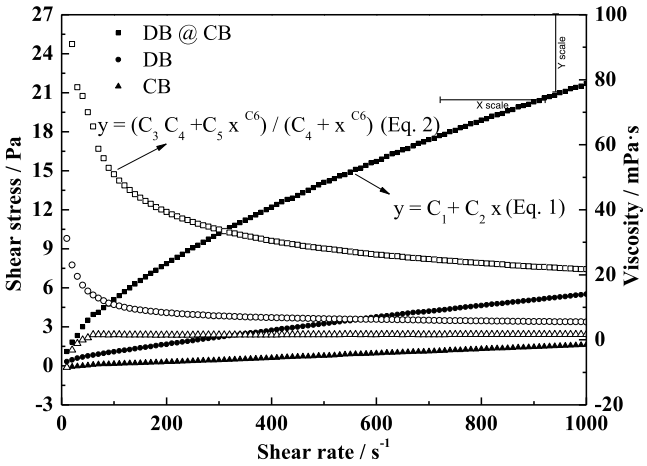

Figure 3. Rheological properties of liquid disperse black dye and carbon black.

It can be seen that the shear stress increased linearly as the shear rate increased in BD, CB, and DB@CB. The relationship between the shear stress (y, Pa) and shear rate (x, s^{-1}) can be described by a linear equation (eq 1) with R^2 near 1 (0.981−0.999), and the viscosity (y, mPa·s) and shear rate (x, s^{-1}) can be described by the Morgan−Mercer−Florin equation (eq 2) with R^2 near 1 (0.993−0.998), as shown in Table 1.

It can be seen by comparing the constants C_1 and C_2 that CB was the smallest, DB@CB was the largest, and DB was between CB and DB@CB. This was because CB was a plastic fluid, C_1 was small (−0.042), and $C_1 + C_2x \approx C_2x$, which was close to the Newtonian liquid, and C_2 was also small (0.002), and the viscosity had the rheological characteristic of shear thickening. CB was a plastic fluid at low shear rates (10−60 s^{-1}) and a Newtonian fluid at high shear rates (60−1000 s^{-1}), with low viscosity values (about 1.6 mPa·s), also confirmed by the high C_4 (965.8) and C_6 (2.455). DB was a pseudoplastic fluid, and C_1 was higher (0.644), but due to the small C_2 (0.005), the linear increase in shear stress with increasing shear rate was smaller. As the shear rate increased, the viscosity of DB decreased rapidly at low shear rates (10−200 s^{-1}), and viscosity changes were smaller when the shear rate continued to increase. Because $C_4 < 0$ and $C_6 < 1$, the viscosity of DB had the rheological characteristic of shear thinning, which indicated that the viscosity decreased rapidly at a low shear rate (10−200 s^{-1}), and the change of viscosity was smaller when the shear rate continued to increase. DB@CB was a typical pseudoplastic fluid, C_1 (0.644) and C_2 (3.829) were the highest, and the linear increase in shear stress with increasing shear rate was great. As the shear rate increased, the viscosity of DB@CB decreased rapidly.

https://doi.org/10.1021/acsomega.2c06993
ACS Omega 2023, 8, 4106−4115

Table 1. Mathematical Model of Shear Stress, Viscosity, and Shear Rate

	eq 1			eq 2				
dye	C_1	C_2	R^2	C_3	C_4	C_5	C_6	R^2
DB	0.644	0.005	0.996	−38956.1	−0.0027	3.492	0.577	0.998
CB	−0.042	0.002	0.999	−11.4	965.8	1.583	2.455	0.993
DB@CB	3.829	0.019	0.981	−593934.3	−0.0004	−8.681	0.304	0.996

Compared to the viscosity of DB and DB@CB, C_4 was very small, $C_4 + x^{C_6} \approx x^{C_6}$, and the Morgan−Mercer−Florin equation (eq 2) can be replaced by a power function mathematical model with R^2 near 1 (0.976−0.994), as shown in Table 2. It was found that as the shear rate increased, the viscosity of DB@CB decreased more significantly than that of DB.

Table 2. Mathematical Model of Viscosity and Shear Rate

dye	mathematical model (power function)	R^2
DB	$y = 71.2 + x^{(-0.389)}$	0.976
DB@CB	$y = 264.7 + x^{(-0.360)}$	0.994

In summary, it can be seen that CB is a plastic fluid with a small-viscosity near-Newtonian fluid, DB is a pseudoplastic fluid with medium viscosity, and DB@CB is a pseudoplastic fluid with high viscosity. The viscosity of liquid dyes consists of structural viscosity and shear viscosity. If the dye or carbon black aggregates are changed, this will enhance the interaction between the dye and carbon black, which will lead to an increase in structural viscosity.

3.2. Aggregation and Interactions of Liquid Disperse Dyes and Carbon Blacks. Figure 4 shows a TEM image of a liquid disperse dye. Figure 4a,b shows a spherical dye aggregate of DO-288 with a particle size of 55−60 nm, and the interaction between the dye and the auxiliaries was visible within the spherical dye aggregate.

Figure 4c shows the dye aggregates of DV-93 (particle size approx. 200−300 nm), which were then aggregated into loose dye aggregates of 800−900 nm by the interaction between the dye and the auxiliaries. Figure 4d shows the dye aggregates of DB-79, which were much looser. Figure 4e,f shows dye aggregates of DB, which were a mixture of dye DO-288, DV-93, and DB-79, forming loose dye aggregates with a particle size of about 1.5−3.0 μm. The above dye aggregates formed a colloidal structure with good dispersion stability.

Figure 5 shows the TEM image of the carbon black. Figure 5a shows the interaction between the nano CB and the additives, and the aqueous nano CB could be uniformly dispersed in the aqueous solution. It was observed that besides the spherical aggregates of CB, lamellar CB aggregates were also present (Figure 5b), which was different from the spherical aggregates of conventional nano CB. The lamellar carbon blacks showed pentagonal (Figure 5c) and hexagonal (Figure 5d−f) aggregates, which were irregular in shape with a maximum length of about 500 nm and a minimum length of about 90 nm. During the mechanical decomposition of CB, in addition to the generation of spherical CB aggregates, there are also a large number of lamellar CB aggregates.

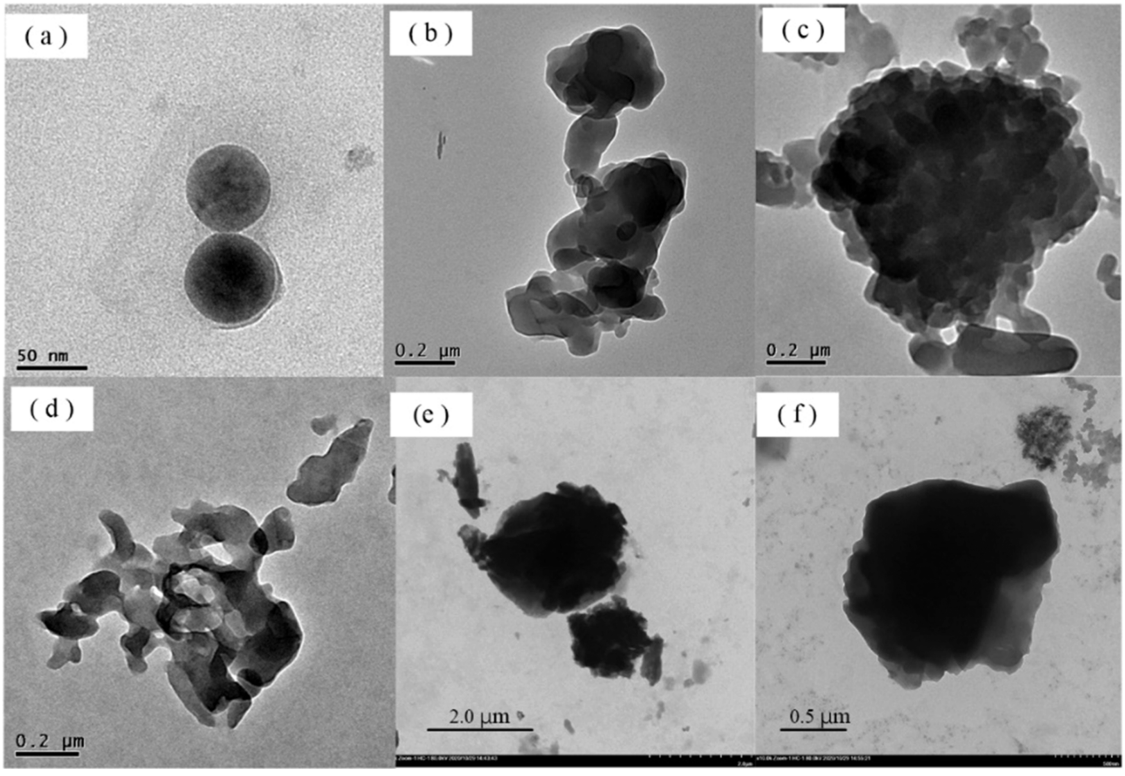

Figure 4. TEM images of liquid disperse dye: (a) DO-288, (b) DO-288, (c) DV-93, (d) DB-79, (e) DB (×4.0k), (f) DB (×10.0k).

https://doi.org/10.1021/acsomega.2c06993
ACS Omega 2023, 8, 4106−4115

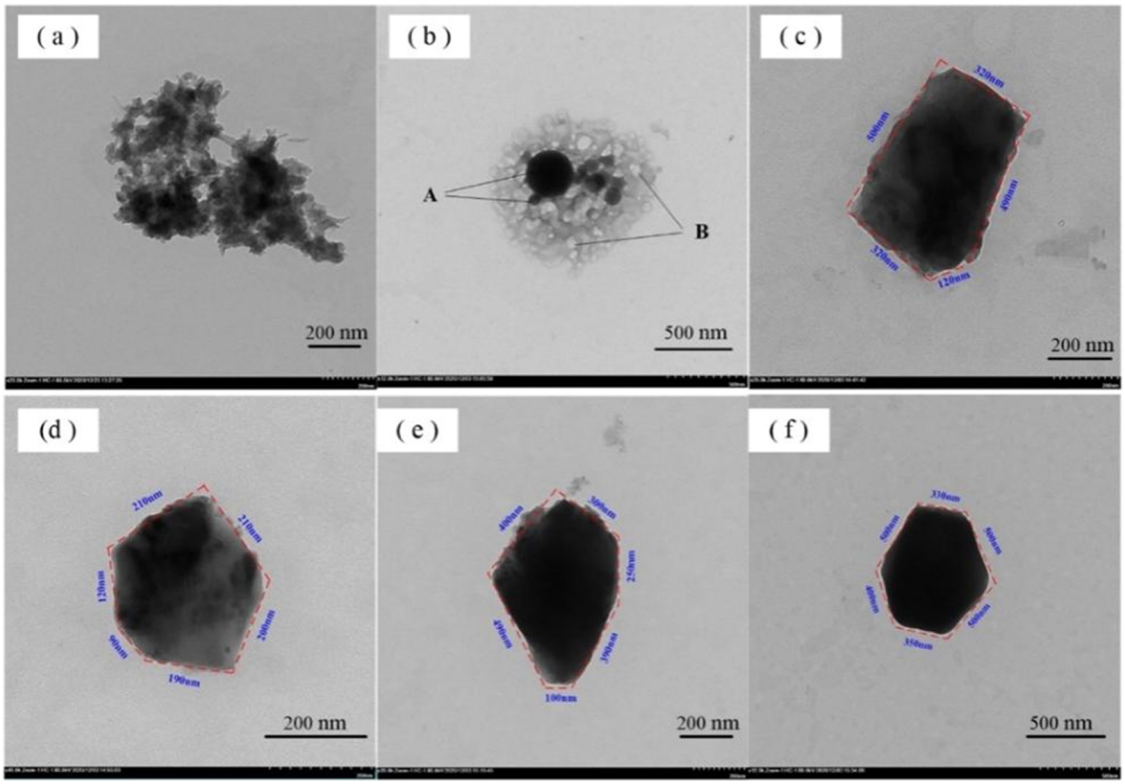

Figure 5. TEM images of liquid CB. Image magnification (a)−(f) was 20.0, 12.0, 40.0, 25.0, 20.0, and 12.0k, respectively.

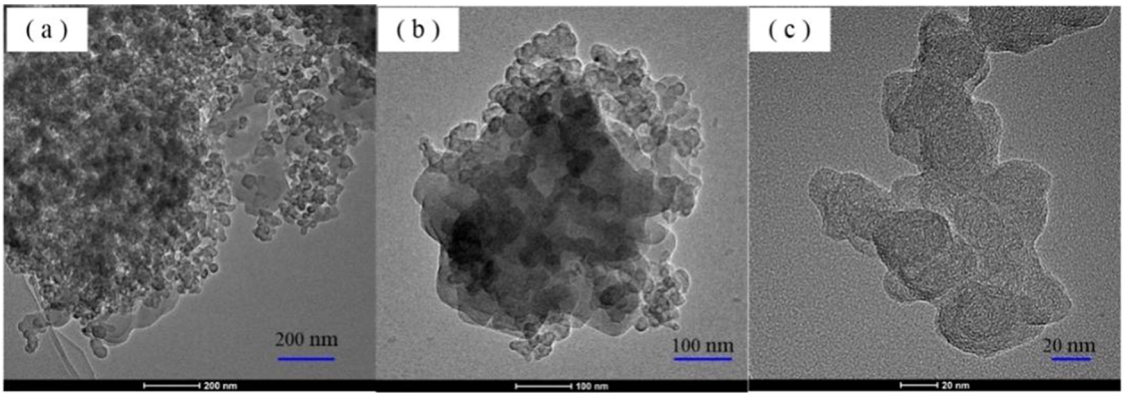

Figure 6. TEM images of liquid DB@CB: (a) 200 nm, (b) 100 nm, (c) 20 nm.

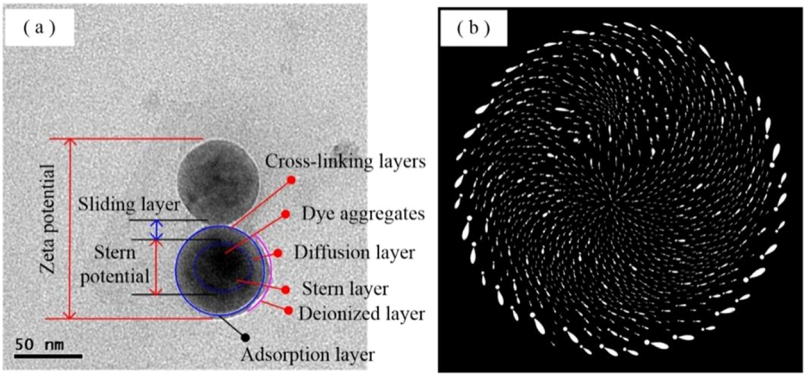

Figure 7. Schematic diagram of stability principle. (a) Liquid dye bilayer diffusion principle and (b) molecular arrangement of liquid DB@CB.

Figure 6 shows the TEM image of DB@CB. Figure 6a shows the presence of larger micelles in DB@CB, which were dyes (DO-288, DV-93, DB-79), CB, and DE 20 forming aggregates containing a large number of nanoscale granular colloids. The

https://doi.org/10.1021/acsomega.2c06993
ACS Omega 2023, 8, 4106−4115

presence of DB@CB colloids with a particle size of about 500−600 nm in DB@CB is shown in Figure 6b, and the process of DB@CB colloid formation is shown in Figure 6c, where the molecular arrangement resembled a vortex-shaped helical curve.

3.3. Stability Analysis of Liquid DB@CB. To describe the interaction between dyes and auxiliaries, a principle of bilayer diffusion was established based on Figure 4a (see Figure 7a).

With high-speed shear and collision, large dye particles can be dispersed into fine particles, even nano-sized particles. In the process of dye particle refinement, the additives can coat the dye particles and form interactions. Due to the interaction between the dye and the surfactant (e.g., electrostatic interaction, H-bonding, van der Waals forces), an adsorption layer (Stern layer) is formed, the potential of which is called Stern potential. The Stern layer can characterize the degree of dye aggregation, depending on the dye particle size, the polarized solvent, and the strength of the counterion. In the outer layer of the dye adsorption layer, it can continue to adsorb surfactants and counterions, forming a diffusion layer of a bilayer (called a sliding layer) and a counterion region, which forms a ζ-potential.

The aggregation of adjacent dyes can form a cross-linking of double electric layers, which can improve the stability of liquid dye micelles when the repulsive forces between dye aggregates prevail, and conversely, dyes have a tendency to aggregate and reduce the stability of dyes (e.g., flocculation, precipitation).[17] Thus, liquid dye stability depends on the adsorption, diffusion, and interaction of dye particles with surfactants, which is a dynamic adsorption−desorption process.

As CB has similar solid characteristics to disperse dyes with weak water solubility, the interaction and stability of CB with surfactants can be explained by the above-mentioned bilayer model of adsorption and diffusion of disperse dyes. In the process of CB mechanical decomposition, DE 20 can improve the stability of liquid CB because it contains good hydrophilic nonionic surfactants. For example, nonionic surfactants (Span 80 and Tween 40) contain −OH, −C═O, and −O−, which can form H-bonds with CB and increase the interaction strength of the Stern adsorption layer and the cross-linked layer of the double electric layer.[18,19]

When the granular CB is in the process of high-speed mechanical deconstruction, mechanical deconstruction force can be due to smaller CB particle size, while the surfactant can form electrostatic and physical adsorption on the surface of CB. CB adsorption of anionic surfactant changes the nature of the charge of the CB particle plasmas in water, which is caused by the strong van der Waals forces between the hydrophobic group of the anionic surface active group and the CB and is an exothermic process.[20−22]

At the same time, the H-bonding of the nonionic surfactants (such as Span 80 and Tween 40) can form a stable mass aggregation of CB particles. Another example is that polyoxymethylene chains can more easily form a solvent water film around the CB, and the movement of polyoxymethylene chains is limited by the presence of H-bonds to produce entropic repulsion, which effectively prevents agglomeration, flocculation, and sedimentation of CB due to its attraction.[23,24]

The lamellar carbon black aggregates are caused by mechanical dissociation force and stable CB aggregates. Due to the strong CB−additive and additive−additive interactions, it can form an aqueous CB fluid that combines lamellar CB and spherical CB.[25,26] Therefore, CB has low viscosity fluidity close to that of a Newtonian fluid.

The molecular arrangement diagram of liquid DB@CB was established based on Figure 6c (see Figure 7b). When DB and CB were present together, strong interactions were formed between DB and CB and the molecular arrangement showed a vortex-shaped helical curve.

Table 3 shows the intermolecular interaction forces between disperse dyes (DV-93, DB-79, DO-288) and CB calculated according to CS Chem 3D Gaussian software. The strong intermolecular attraction of three disperse dyes was −122.136 (DV-93), −26.871 (DB-79), and −111.068 (DO-288) kJ/mol, respectively. Therefore, in the liquid disperse dye black (DB), the intermolecular attraction of the dyestuff was higher than the repulsion, and DB showed a strong intermolecular attraction. The CB intermolecular repulsive force was higher than the attractive force, which showed a strong intermolecular repulsive force. When both CB and DB coexist, there is a strong interaction between DB and CB molecules, which is beneficial to the stability of the liquid DB@CB and results in the rheology of DB@CB with plastic fluid properties. This may explain the appearance of a vortex-shaped helical molecular arrangement between CB and DB molecules.

Table 3. Intermolecular Forces of Disperse Dyes and Carbon Black

	DB			
forces (kJ/mol)	DV-93	DB-79	DO-288	CB
stretch	57.641	60.732	40.576	19.663
bend	83.260	131.897	75.062	66.230
stretch-bend	−119.067	−127.637	−106.902	0.590
torsion	−91.678	−94.883	−134.074	−1.986
non-1,4 VDW	−18.563	−26.984	−22.826	−39.705
1,4 VDW	17.082	59.545	35.846	146.652
charge/charge	−14.647	−23.223	0	0
charge/dipole	−16.870	−18.035	1.164	0
dipole/dipole	−19.294	11.719	0.086	3.252
total of repulsion	157.984	263.892	152.733	236.387
total of attraction	−280.120	−290.762	−263.801	−41.691
total	−122.136	−26.871	−111.068	194.696

3.4. Conductivity of Fabrics Using Liquid DB@CB. Figure 8a shows the relationship between DB@CB concentration and resistance in the warp direction of the fabric. As the concentration of DB@CB increased, the resistance of the fabric decreased significantly, with resistances of 66.7 MΩ (8%), 13.0 MΩ (12%), 463.2 kΩ (20%), 308.9 kΩ (30%), respectively. Figure 8b shows the effect of DB@CB concentration on resistance in the warp direction of the fabric by 30% stretched. The stretch fabric increased the resistance by 405.9 MΩ (8%), 34.9 MΩ (12%), 1.9 MΩ (20% CB), and 734.1 kΩ (30% CB), respectively. Figure 8c shows the effect of DB@CB concentration on resistance in the weft direction of the fabric by 0 and 30% stretched. As the concentration of DB@CB increased, the resistance decreased significantly. Similar to the fabric warp direction, the weft direction was stretched and increased the fabric resistance. Resistance increased by 6.3 MΩ (8%), 0.2 MΩ (12%), 84.0 kΩ (20%), and 17.0 kΩ (30%), respectively, after 30% stretching of the fabric. During the stretching process, the resistance of the conductive fabric shows an increasing change, which indicates

https://doi.org/10.1021/acsomega.2c06993
ACS Omega 2023, 8, 4106−4115

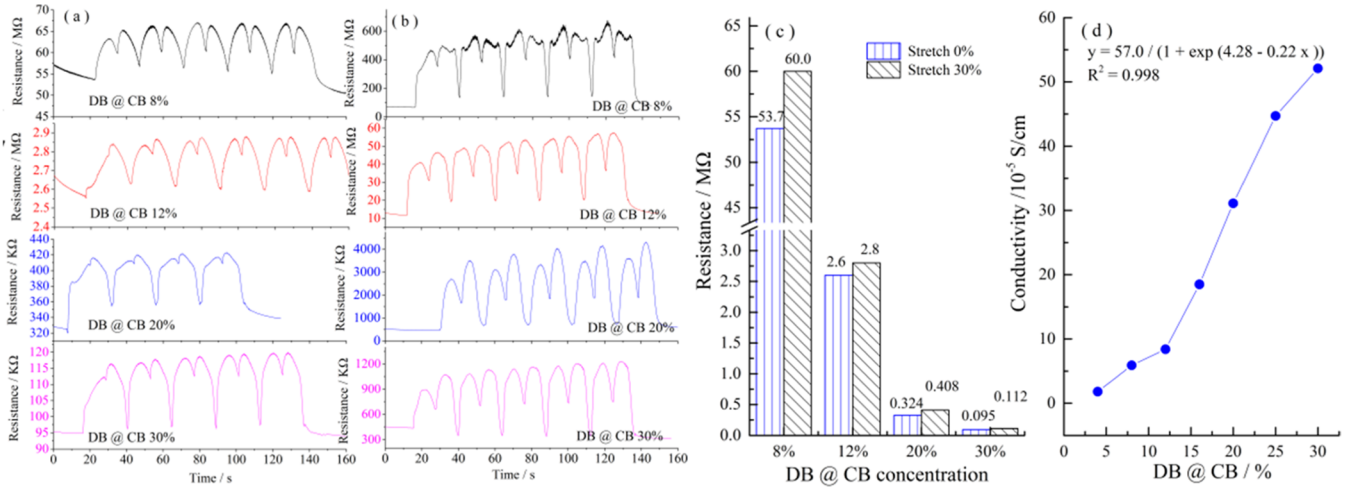

Figure 8. Effect of DB@CB concentration on fabric resistance and electrical conductivity. (a) Fabric warp resistance (Unstretched), (b) fabric warp resistance (Stretched 30%), (c) fabric weft resistance, (d) fabric conductivity.

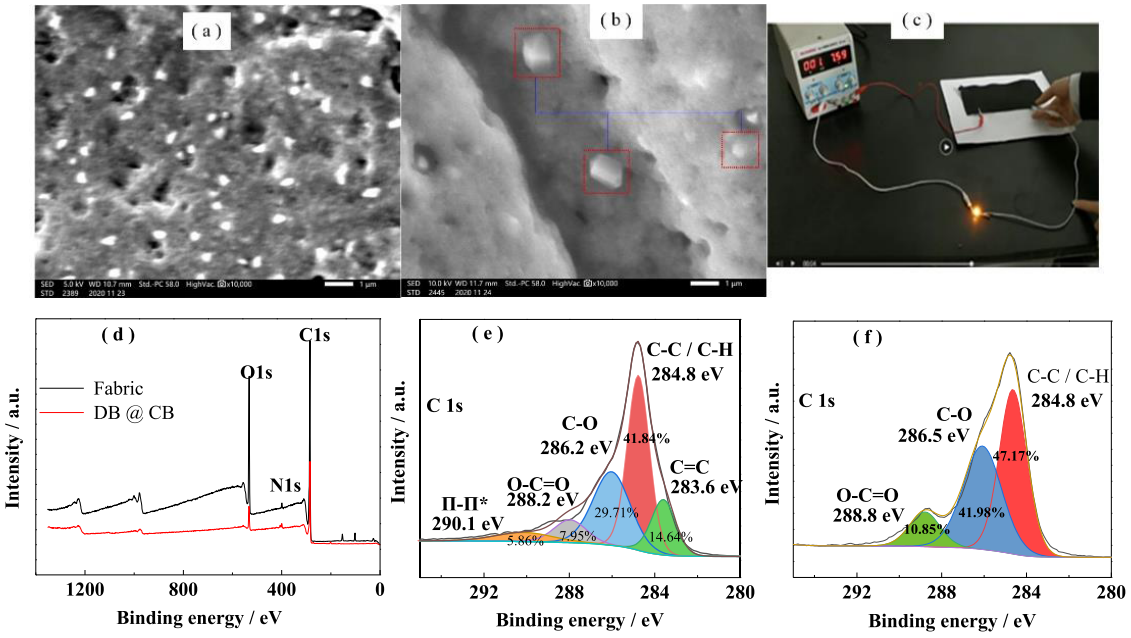

Figure 9. Surface properties of DB@CB dyed fibers. (a, b) SEM of DB@CB dyed fabric (×10.0k). (c) Electrical conductivity of DB@CB dyed fabric. (d) XPS of polyester/spandex fabric and DB@CB dyed fabric. (e) High-resolution C 1s XPS spectra of polyester/spandex fabric. (f) High-resolution C 1s XPS spectra of DB@CB dyed fabric.

that the CB-film aggregated on the surface of the fibers has good stretching properties and that the conductive CB has good strain-sensing behaviors. This decrease in resistance depends mainly on the difference in the microstructure of the conductive filler and the interaction between the filler and the substrate.[27]

Figure 8d shows the effect of DB@CB concentration on conductivity. As the concentration of DB@CB increased, the resistance decreased significantly and the conductivity increased. The variation of fabric conductivity (y, $\times 10^{-5}$ S/cm) with DB@CB (x, %) concentration can also be described by a logistic model with R^2 near 1 (0.998), $y = 57.0/[1 + \exp(4.28-0.22x)]$, as shown in Figure 8d. It is shown in the logistic model that when the concentration of DB@CB on the fabric is low, the conductivity increases significantly by increasing the concentration of DB@CB, and the conductivity no longer increases significantly with increasing concentration of DB@CB.

In this test, a uniform carbon black aggregation layer can be formed on the fiber surface with uniform fine pore structure and crystallization on the fiber surface (see Figure 9a,b). The excellent conductivity of the fiber depends on the three-dimensional continuous conductive network layer,[28] and the structure and performance of the CB-film aggregation as well as the thickness of the conductive network layer have less influence on the electrical conductivity. In addition, the effect of additives (surfactants, binders) in aqueous CB emulsions has a limited effect on the conductivity of the CB.[5] The aggregated CB-film on the surface of the fabric is an anisotropic conductive film, which can be obtained by shear flow-induced assembly of the carbonaceous filler,[29] and by the induced assembly of the warp and weft yarns of the fabric in

https://doi.org/10.1021/acsomega.2c06993
ACS Omega 2023, 8, 4106−4115

Table 4. Dyeing Properties of Fabrics Using Liquid DB@CB

	color characteristic			color fastness/grade				
				rubbing		washing		
DB@CB (%)	L^*	a^*	b^*	dry	wet	change	staining	electrical conductivity ($\times 10^{-5}$ S/cm)
5	16.52 ± 0.14	0.73 ± 0.06	−1.16 ± 0.18	4−5	4−5	4−5	4−5	2.9
10	15.48 ± 0.12	0.85 ± 0.05	−1.18 ± 0.15	4	4	4−5	4−5	6.8
20	15.20 ± 0.16	0.86 ± 0.04	−1.20 ± 0.11	3−4	3−4	4	4	31.1

this test. For example, the resistance in the warp of the polyester/spandex fabric was significantly higher than the resistance in the weft. The surface of the fabric formed an orderly arrangement of CB crystals, both spherical structured crystals and polygonal block crystals with a particle size of about 200−500 nm (Figure 9b). Such block crystals have not been reported and may be related to the presence of various lamellar CB aggregates in the liquid CB. The lamellar carbon black aggregates dominate the formation and growth of block crystal structures.

The polyester/spandex fabric of DB@CB had excellent electrical conductivity (3.1×10^{-4} S/cm, 20% DB@CB), which can light up a light bulb as a circuit conductor (see Figure 9c). The XPS spectra of the polyester/spandex fabric and DB@CB dyed fabric are shown in Figure 9d−f. The elemental compositions of samples polyester/spandex and DB@CB were similar, and only the elemental content was different. The main element was C (284.7 eV, C 1s), N (399.0 eV, N 1s), and O (532.6 eV, O 1s). The C 1s of the sample polyester/spandex corresponds to C−C/C−H (284.8 eV), C−O (286.5 eV), and O−C═O (288.8 eV), and the C 1s of the sample DB@CB corresponds to C−C/C−H (284.8 eV), C−O (286.2 eV), O−C═O (288.2 eV), C═C (283.6 eV), and $\pi-\pi^*$ (290.1 eV), where C═C and $\pi-\pi^*$ are the peaks of CB.

The equivalent spheres of CB aggregate as basic units to describe the nonlinear conductive behavior have drawbacks and do not explain the conductive mechanism of block crystal structures.[30] In this test, we have observed many lamellar CB aggregates, block crystal structures, aqueous CB with near Newtonian fluids, a vortex-shaped helical molecular arrangement, and $\pi-\pi^*$ intermolecular interactions (peak area of 5.86%). Therefore, it is believed that a two-dimensional carbon structure exists in the liquid DB@CB. The excellent dispersion and stability of the CB in the finishing solution facilitate the formation of effective conductive paths and the generation of a stable electrical signal with a higher conductivity.[31,32] In addition, the lamellar carbon black may be a two-dimensional carbon structure, and the existence of flat bands in two-dimensional carbon quantum materials, in which the electrons interact strongly with each other, can produce special electrical properties.[33] In contrast, block crystals may have an intrinsic misalignment stacking that causes near-electron flat bands to appear on the surface of block crystals, the mechanism of which is related to the quantum spin Hall effect,[34] significantly enhancing conductivity.

3.5. Dyeing Properties of Fabrics Using Liquid DB@CB. Table 4 shows the effect of DB@CB concentration on the dyeing properties of polyester/spandex fabrics. It could be seen that as the DB@CB concentration increased, the electrical conductivity increased, the black depth increased, and the black fabric showed a slight reddish-bluish color. When the concentration of DB@CB was 5%, the rubbing and washing color fastness were excellent (with 4−5). Continuing to increase the concentration of DB@CB, it also had good color fastness, with rubbing and washing color fastness reaching 3−4 and 4 grades, respectively, which can meet the requirements of color fastness of textile garments.

This is because a uniform CB film can form on the fabric surface, and when the black depth reaches a certain value, even if a thicker CB film is formed, the effect on the color depth is smaller.

Under high-temperature baking conditions, the disperse dye on the surface of the fabric diffuses, penetrates, and fixes inside the fiber, so DB@CB can produce dark black fabrics with excellent fastness and good electrical conductivity. The processing method of pad-dry-bake is both simple and economical, and the process has no wastewater emission.

4. CONCLUSIONS

In this study, liquid carbon black and disperse dye black (DB@CB) are prepared. It is used to dye polyester/spandex fabrics with a short process of dip-dry-bake method. The fabric has the properties of deep black color, excellent color fastness, and good electrical conductivity. Liquid carbon black has the characteristics of a near-Newtonian fluid, showing repulsive forces between carbon black molecules, while liquid dispersion black alone shows the characteristics of a plastic fluid, showing attractive forces between dye molecules. Due to the strong interaction between carbon black and disperse dye, there are vortex-shaped helical molecular arrangement and two-dimensional lamellar structure between liquid DB@CB molecules, showing pseudoplastic fluid characteristics, and its viscosity and shear rate accord with Morgan−Mercer−Florin and power function mathematical models. Therefore, liquid DB@CB has excellent stability.

The polyester/spandex fabric dyed with liquid DB@CB has low resistance and can even light up a light bulb, and its electrical conductivity and DB@CB concentration are by the logistic model mathematical model. Its excellent electrical conductivity is related to the ordered arrangement of carbon black aggregates, block crystals, and $\pi-\pi^*$ intermolecular interactions. DB@CB dyed polyester/spandex fabrics have the advantage of deep black color, excellent color fastness, and rubbing and washing color fastness of not less than 3−4.

The modified carbon black method provided in this study is both practical and economical to meet the garment requirements of conductive textiles, and the process has no wastewater emission, which can find new uses for carbon black modification.

AUTHOR INFORMATION

Corresponding Author

Hongmei Cao − *Changzhou Vocational Institute of Textile and Garment, Changzhou, Jiangsu 213164, China;* orcid.org/0000-0003-1195-6414; Email: hmcao@cztgi.edu.cn

https://doi.org/10.1021/acsomega.2c06993
ACS Omega 2023, 8, 4106−4115

Authors

Li Ai − *State Key Laboratory of New Textile Materials and Advanced Processing Technologies, Wuhan Textile University, Wuhan 430200, China;* orcid.org/0000-0001-8574-5412

Shanshan Li − *College of Textile and Clothing Engineering, Soochow University, Suzhou, Jiangsu 215021, China*

Yawei Zhu − *College of Textile and Clothing Engineering, Soochow University, Suzhou, Jiangsu 215021, China*

Complete contact information is available at: https://pubs.acs.org/10.1021/acsomega.2c06993

Funding

The authors disclosed receipt of the following financial support for the research, authorship, and/or publication of this article: This study was funded by Natural Science Research Projects in Colleges and Universities of Jiangsu Province (21KJA540003), Science and Technology Innovation Team Project of Changzhou Vocational Institute of Textile and Garment (CFTD202103), and Changzhou Science and Technology Support Program (Social Development) (CE20225004).

Notes

The authors declare no competing financial interest.

The authors declared no potential conflicts of interest with respect to the research, authorship, and/or publication of this article.

■ ACKNOWLEDGMENTS

The authors declare that they have no competing financial interests or personal relationships.

■ REFERENCES

(1) Yadav, R.; Tirumali, M.; Wang, X.; Naebe, M.; Kandasubramanian, B. Polymer composite for antistatic application in aerospace. *Def. Technol.* **2020**, *16*, 107−118.

(2) Kang, L.; Du, H. L.; Du, X.; Wang, H. T.; Zhang, F. B.; et al. Study on dye wastewater treatment of tunable conductivity solid-waste-based composite cementitious material catalyst. *Desalin. Water Treat.* **2018**, *125*, 296−301.

(3) Wen, J. Q.; Xie, J.; Yang, Z. H.; Shen, R.; Li, H.; Li, X. Y.; Luo, X. B.; Chen, X. B.; Li, X. Fabricating the robust g-C3N4 nanosheets/carbons/NiS multiple heterojunctions for enhanced photocatalytic H-2 generation: an insight into the trifunctional roles of nanocarbons. *ACS Sustainable Chem. Eng.* **2017**, *5*, 2224−2236.

(4) Gu, J.; Héroguel, F.; Luterbacher, J.; Hu, X. L. Densely packed, ultra small SnO nanoparticles for enhanced activity and selectivity in electrochemical CO_2 reduction. *Angew. Chem., Int. Ed.* **2018**, *57*, 2943−2947.

(5) Marinho, B.; Ghislandi, M.; Tkalya, E.; Koning, C. E.; With, G. D. Electrical conductivity of compacts of graphene, multi-wall carbon nanotubes, carbon black, and graphite powder. *Powder Technol.* **2012**, *221*, 351−358.

(6) Thomassin, J. M.; Christine, J.; Pardoen, T.; Bailly, C.; Huynen, I.; Detrembleur, C. Polymer/carbon based composites as electromagnetic interference (EMI) shielding materials. *Mater. Sci. Eng., R* **2013**, *74*, 211−232.

(7) Ghosh, S.; Remanan, S.; Mondal, S.; Ganguly, S.; Das, P.; Singha, N.; Das, N. C. An approach to prepare mechanically robust full IPN strengthened conductive cotton fabric for high strain tolerant electromagnetic interference shielding. *Chem. Eng. J.* **2018**, *344*, 138−154.

(8) Li, G. C.; Li, G. R.; Ye, S. H.; Gao, X. P. A polyaniline-coated sulfur/carbon composite with an enhanced high-rate capability as a cathode material for lithium/sulfur batteries. *Adv. Energy. Mater.* **2012**, *2*, 1238−1245.

(9) Lu, N. S.; Lu, C.; Yang, S. X.; Rogers, J. Highly sensitive skin-mountable strain gauges based entirely on elastomers. *Adv. Funct. Mater.* **2012**, *22*, 4044−4050.

(10) Wu, X. D.; Han, Y.; Zhang, X.; Zhou, Z. H.; Lu, C. H. Large-area compliant, low-cost, and versatile pressure-sensing platform based on microcrack-designed carbon black@polyurethane sponge for human-machine interfacing. *Adv. Funct. Mater.* **2016**, *26*, 6246−6256.

(11) Zheng, Y. J.; Li, Y. L.; Dai, K.; Wang, Y.; Zheng, G. Q.; Liu, C. T.; Shen, C. Y. A highly stretchable and stable strain sensor based on hybrid carbon nanofillers/polydimethylsiloxane conductive composites for large human motions monitoring. *Compos. Sci. Technol.* **2018**, *156*, 276−286.

(12) Zheng, Y. J.; Li, Y. L.; Li, Z.; Wang, Y. L.; Dai, K.; Zheng, G. Q.; Liu, C. T.; Shen, C. Y. The effect of filler dimensionality on the electromechanical performance of polydimethylsiloxane based conductive nanocomposites for flexible strain sensors. *Compos. Sci. Technol.* **2017**, *139*, 64−73.

(13) Thomassin, J. M.; Christine, J.; Pardoen, T.; Bailly, C.; Huynen, I. C. Detrembleur. Polymer/carbon based composites as electromagnetic interference (EMI) shielding materials. *Mater. Sci. Eng., R* **2013**, *7*, 211−232.

(14) Keshavarz, A. H.; Mohseni, M.; Montazer, M. Electroconductive modification of polyethylene terephthalate fabric with nano carbon black and washing fastness improvement by dopamine self-polymerized layer. *J. Appl. Polym. Sci.* **2019**, *136*, 48035.

(15) Hu, C. C.; Chang, S. S.; Liang, N. Y. Fabrication and characterization of antistatic fiber with segmented pie structure. *Text. Res. J.* **2016**, *86*, 1828−1836.

(16) Choi, H. J.; Kim, M. S.; Ahn, D.; Yeo, S. Y.; Lee, S. Electrical percolation threshold of carbon black in a polymer matrix and its application to antistatic fibre. *Sci. Rep.* **2019**, *9*, No. 6338.

(17) Makarewicz, E.; Michalik, A. Research on the influence of the type of surfactant and concentrator in aqueous dispersion of pigments. *J. Surfactants Deterg.* **2014**, *17*, 773−784.

(18) Zhao, Y. P.; Lu, P.; Li, C. K.; Fan, X. P.; Wen, Q. B.; Zhan, Q.; Shu, X.; Xu, T. L.; Zeng, G. M. Adsorption mechanism of sodium dodecyl benzene sulfonate on carbon blacks by adsorption isotherm and zeta potential determinations. *Environ. Technol.* **2013**, *34*, 201−207.

(19) Dwivedi, C.; Mohanty, T. R.; Manjare, S. D.; Rajan, S. K.; Ramakrishnan, S.; Amarnath, S. K. P.; Lorenzetti, D.; Mohamed, P. K. Application of non-ionic surfactant in modifying the surface of carbon black and its role in the formation of colloidal composite materials. *Colloids Surf., A* **2021**, *624*, No. 126825.

(20) Sis, H.; Birinci, M. Effect of nonionic and ionic surfactants on zeta potential and dispersion properties of carbon black powders. *Colloids Surf., A* **2009**, *341*, 60−67.

(21) Kochkodan, O.; Maksin, V.; Semenenko, T. Adsorption of sodium hexadecyl sulfate and triton X from binary aqueous solutions at thermally graphitized carbon black. *Period. Polytech., Chem. Eng.* **2020**, *65*, 72−79.

(22) González-García, C.; González-Martín, M. L.; Denoyel, R.; Gallardo-Moreno, A. M.; Labajos-Broncano, L.; Bruque, J. M. Adsorption enthalpies of sodium dodecyl sulphate onto carbon blacks in the low concentration range. *Carbon* **2005**, *43*, 567−572.

(23) González-García, C. M.; González-Martín, M. L.; Gómez-Serrano, V.; Bruque, J. M.; Labajos-Broncano, L. Determination of the free energy of adsorption on carbon blacks of a nonionic surfactant from aqueous solutions. *Langmuir* **2000**, *16*, 3950−3956.

(24) Gupta, S. D.; Bhagwat, S. S. Adsorption of surfactants on carbon black-water interface. *J. Dispersion Sci. Technol.* **2005**, *26*, 111−120.

(25) Santini, E.; Ravera, F.; Ferrari, M.; Alfè, M.; Ciajolo, A.; Liggieri, L. Interfacial properties of carbon particulate-laden liquid interfaces and stability of related foams and emulsions. *Colloids Surf., A* **2010**, *365*, 189−198.

(26) Liu, X. H.; Zhao, Y.; Liu, Z.; Wang, D. J.; Xu, D. F. Preparation and characterization of modified nano carbon black/polyurethane composites. *Chem. J. Chin. Univ.* **2008**, *29*, 2096−2100.

(27) Zhao, J.; Dai, K.; Liu, C.; Zheng, G.; Wang, B.; Liu, C.; Chen, J.; Shen, C. A comparison between strain sensing behaviors of carbon black/polypropylene and carbon nanotubes/polypropylene electrically conductive composites. *Composites, Part A* **2013**, *48*, 129−136.
(28) Hong, R.; Zhao, Z. H.; Leng, J.; Wu, J. J.; Zhang, J. Two-step approach based on selective laser sintering for high performance carbon black/polyamide 12 composite with 3D segregated conductive network. *Composites, Part B* **2019**, *176*, No. 107214.
(29) Huang, J.; Xu, J.; Sheng, Y.; Zhu, Y.; Jiang, W.; Xu, D.; Tang, Q.; Nie, X. Fabrication of polymer film with extraordinary conductive anisotropy by forming parallel conductive vorticity-aligned stripes and its formation mechanism. *Macromol. Mater. Eng.* **2016**, *301*, 743−749.
(30) Liang, J.; Yang, Q. Aggregate structure and percolation behavior in polymer/carbon black conductive composites. *J. Appl. Phys.* **2007**, *102*, No. 083508.
(31) Liu, H.; Huang, W. J.; Yang, X. R.; Dai, K.; Zheng, G. Q.; Liu, C. T.; Shen, C. Y.; Yan, X. R.; Guo, J.; Guo, Z. H. Organic vapor sensing behaviors of conductive thermoplastic polyurethane-graphene nanocomposites. *J. Mater. Chem. C* **2016**, *4*, 4459−4469.
(32) Yasin, S.; Luckham, P. F.; Iqbal, T.; Zafar, M.; Ramzan, N. Adsorption and rheology of graphitic carbon black nonaqueous dispersions prepared using nonionic surfactants. *J. Dispersion Sci. Technol.* **2013**, *34*, 737−746.
(33) Mao, J.; Milovanović, S. P.; Anđelković, M.; Lai, X.; Cao, Y.; Watanabe, K.; Taniguchi, T.; Covaci, L.; Peeters, F. M.; Geim, A. K.; et al. Evidence of flat bands and correlated states in buckled graphene superlattices. *Nature* **2020**, *584*, 215−220.
(34) Shi, Y.; Xu, S.; Yang, Y.; Slizovskiy, S.; Mishchenko, A.; et al. Electronic phase separation in multilayer rhombohedral graphite. *Nature* **2020**, *584*, 210−214.

https://doi.org/10.1021/acsomega.2c06993
ACS Omega 2023, 8, 4106−4115